Supplementary Information for

Ultra-effective room temperature gas discrimination based on monolithic Pd@MOF-derived porous nanocomposites: An exclusive scheme with photoexcitation

Peiyu Duan,[a] Haowen Wang,[a] Qingkui Peng,[a] Hongmin Zhou,[b] Qiangling Duan,[a] Kaiqiang Jin,*[a] and Jinhua Sun*[a]

[a]*State Key Laboratory of Fire Science, University of Science and Technology of China, No.96 JinZhai Road, Hefei, Anhui, 230026, People's Republic of China*

[b]*Physical and Chemical Science Experiment Center, University of Science and Technology of China, No.96 JinZhai Road, Hefei, Anhui, 230026, People's Republic of China*

** Corresponding authors: E-mail: jinkq@ustc.edu.cn, sunjh@ustc.edu.cn*

Contents

Supplementary Note 1 | Materials

Materials. The methanol (MeOH), zinc nitrate hexahydrate ($Zn(NO_3)_2 \cdot 6H_2O$), Palladium chloride ($PdCl_2$), and Polyvinylpyrrolidone (PVP, K30) were purchased from Sinopharm Chemical Reagent Co. Ltd. The 2-Methylimidazole (2-MeIM, 99%) was purchased from J&K Scientific Co. Ltd. All the chemical reagents used for the synthesis of MOF-derived xPd@ZnO porous nanocomposites were analytical grade.

Supplementary Note 2 | Characterization of materials

Characterization. The X-ray diffraction (XRD) with Cu Kα1 radiation (λ = 1.5406 Å) were employed to investigate the composition and crystal structure of the nanocomposites. The valence states and elemental compositions were characterized by X-ray photoelectron spectroscopy (XPS, ESCLAB 250Xi) and X-ray spectrometer (EDX, Gemini SEM 500). The microstructure and morphology characterizations were carried out by the transmission electron microscopy (TEM, JEM2100 F) and the scanning electron microscopy (SEM, Gemini SEM 500). The analysis of N_2 adsorption-desorption isothermal were performed to explore the porous structures of the nanocomposites by Brunauer-Emmett-Teller method (BET, Tristar II 3020 M). The UV–vis absorbance spectra were studied by the Uv-Visible-Near infrared spectrophotometer (Solid 3700 DUV). The high-angle annular dark-field scanning transmission electron microscope (HAADF-STEM) characterizations and the corresponding EDS elemental mapping of MOF-derived 5.0Pd@ZnO nanocomposites were conducted on Spherical Aberration Corrected Transmission Electron Microscope (Themis Z, Thermal Fisher).

Supplementary Note 3 | PCA Pattern Recognition Methods

PCA Pattern Recognition Methods. The recognition of the gases was realized by principal component analysis methods. In the actual process, the dimensionality reduction and classification of signals are usually completed according to the response characteristics obtained from sensor arrays or multiple experiments. In this experiment, the PCA pattern recognition was mainly implemented through a sensor array prepared based on MOF-derived 5.0Pd@ZnO nanocomposites. The gas identification process was completed by analyzing the response behavior characteristics of the sensing array composed of three similar sensors to the same type of gas. This method aimed to provide a feasible reference for subsequent gas identification researches of related fields. In the future, the response characteristics of the arrays composed of different sensors and the large number of data samples can be used to achieve more accurate gas identification. In this work, the details of the PCA pattern recognition method are as follows:

a) Firstly, discretize the characteristic original data such as multiple response values, response characteristics, recovery characteristics, and gas concentrations obtained by the sensing array to each gas, and generated a matrix *X* of m (rows) × n (columns). In this work, a sensing array composed of 3 sensors was selected to test 9 kinds of gases, resulting in a 27×4 discretized matrix *X*.

b) Decentralize the data and subtract its own average value from each feature. The calculation method is as follows:

$$\bar{x} = \frac{1}{n}\sum_{i=1}^{n} x_i \quad (1)$$

$$S^2 = \frac{1}{n-1}\sum_{i=1}^{n}(x_i - \bar{x})^2 \quad (2)$$

c) Calculate the covariance matrix of the sample $\frac{1}{n}XX^T$. The calculation method is as follows:

$$cov(X,Y) = \frac{\sum_{i=1}^{n}(X_i-\bar{X})(Y_i-\bar{Y})}{n-1} \quad (3)$$

d) Use the eigenvalue decomposition method to find the eigenvalues and eigenvectors of the covariance matrix. The eigenvectors were arranged in rows from top to bottom into a matrix *P* according to the corresponding eigenvalues. In this experiment, the main eigenvalues were 2.64 and 1.28, accounting for 66.09% and 32.12%, respectively.

e) Finally, the dimensionality of the original experimental data was reduced to a new two-dimensional matrix Y ($Y=PX$). The PCA pattern recognition shown in Figure 4e was final obtained after the visualization with a 95% confidence interval.

Supplementary Note 4 | DFT Computational Methods

DFT Computational Methods. The DFT based on generalized gradient approximation was used to perform the periodic calculations, which employed the Perdew-Burke-Ernzerhof exchange-correlation functional as implemented in the plane-wave program Vienna ab initio simulation package (VASP).[1, 2] The core electron representation adopted the projector-augmented wave potentials.[3] The cutoff energy of the plane wave is 500 eV and 400 eV for systems with and without Pd atom, respectively. The integration in the reciprocal space was performed with a Monkhorst−Pack grid. A k-point mesh of (9 × 9 × 5) was used for relaxation of ZnO primitive cell. Accordingly, and a (5 × 3) supercell of ZnO (10−10) surface was established with a vacuum layer of 15 Å. The bottom two Zn-O layers were fixed to simulate bulk atoms, while the other six layers could be relaxed. Single gamma point was used for further surface simulation. The geometries are fully relaxed with all forces < 0.02 eV/Å.

There are 120 Zn atoms and 120 O atoms in the supercell. According to experiments, other three MOF-derived xPd@ZnO surfaces were established. It was supposed that Pd was embedded into lattice with low Pd content and Pd cluster was formed with high Pd content. The adsorption behavior of O_2 and H_2 was then simulated at these surfaces. The adsorption energy (E_{ads}) is defined as following equation:

$$E_{ads} = E_{surface+molecule} - E_{surface} - E_{molecule}$$

The $E_{surface+molecule}$ is the energy of the surface adsorbed with molecule; the $E_{surface}$, $E_{molecule}$ represents energy of surface and single molecule. Notably, several possible configurations were considered for each adsorption, and the one presented here was the most stable structure. Bader charge was also analyzed for these adsorption configurations.[4] The unit of Bader charge is elemental electron charge e, thus the negative value means extracting electron from surface.

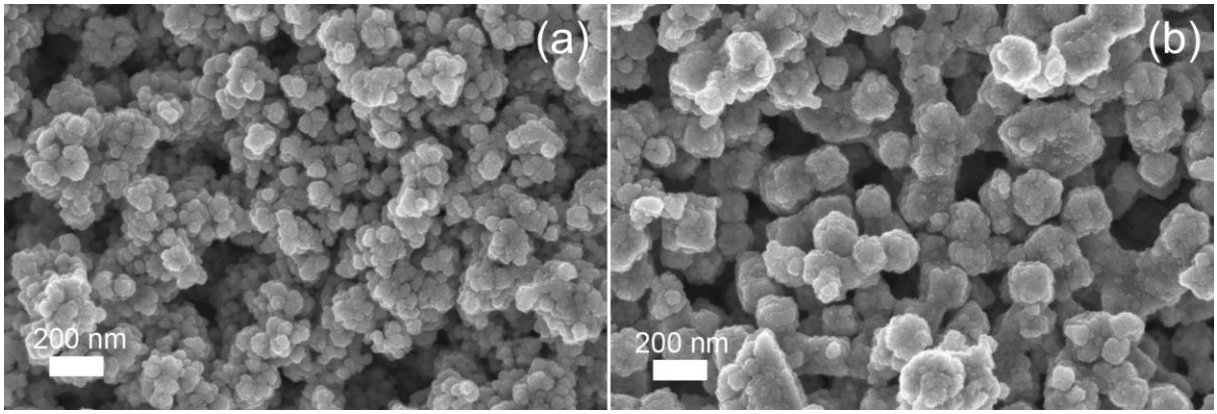

Figure S1. SEM image of the ZIF-8-based materials directly sintered in air at 400 ℃: a) Pure ZIF-8 and b) 5.0Pd@ZIF-8 nanocomposites.

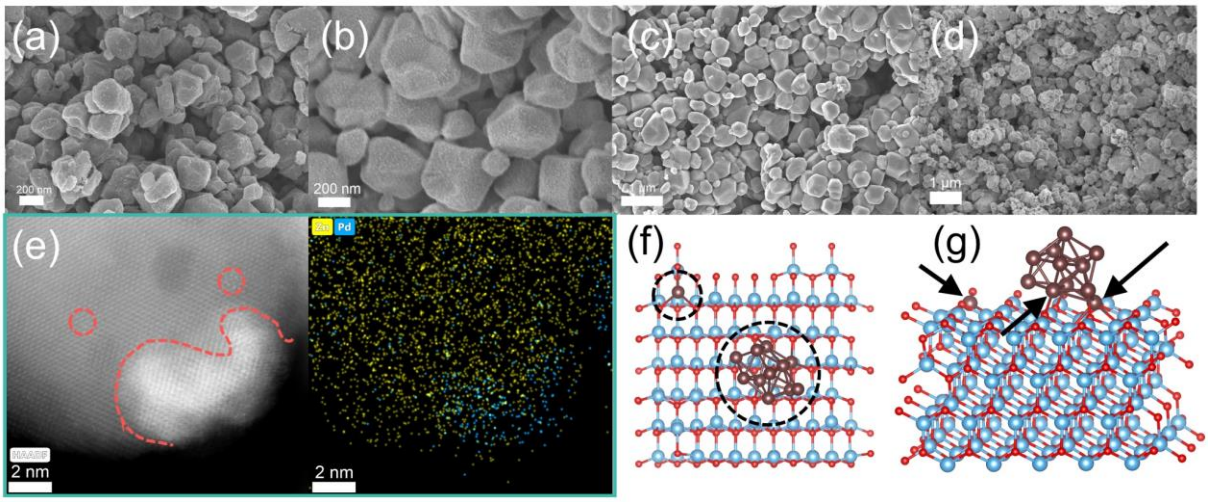

Figure S2. Morphology variation characterization and the Pd states clarification of the MOF-derived nanocomposites. a) Carbonized MOF-derived 2.5Pd@ZIF-8; b) annealed MOF-derived 2.5Pd@ZnO; c) Carbonized MOF-derived 5.0Pd@ZIF-8; d) annealed MOF-derived 2.5Pd@ZnO; e) HAADF-STEM image and EDS elemental mapping of 5.0Pd@ZnO; f) top view of the simulation model of MOF-derived 10.0Pd@ZnO; g) Growth preference of Pd nanoclusters on the surface of materials.

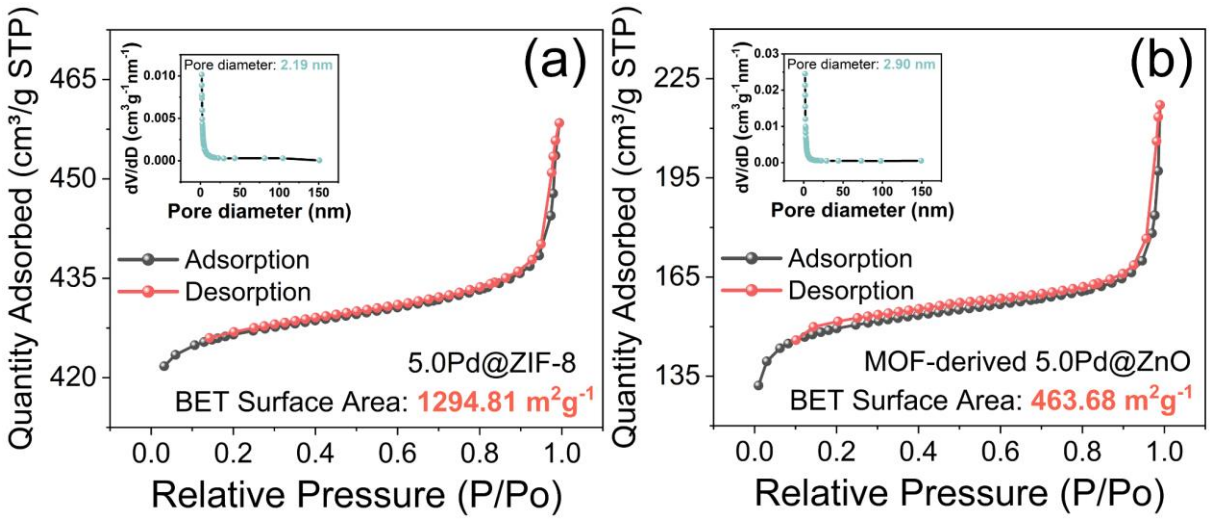

Figure S3. N_2 adsorption-desorption isotherms of (a) 5.0Pd@ZIF-8 and (b) 5.0Pd@ZnO porous nanocomposites.

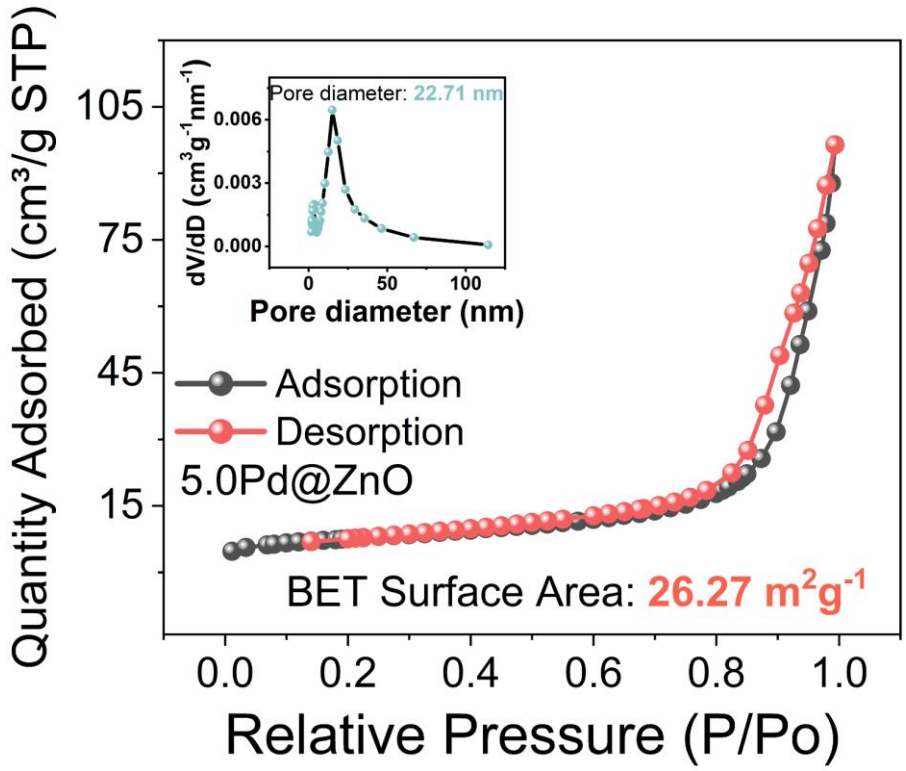

Figure S4. N_2 adsorption-desorption isotherms of 5.0Pd@ZnO obtained from 5.0Pd@ZIF-8 sintered in air.

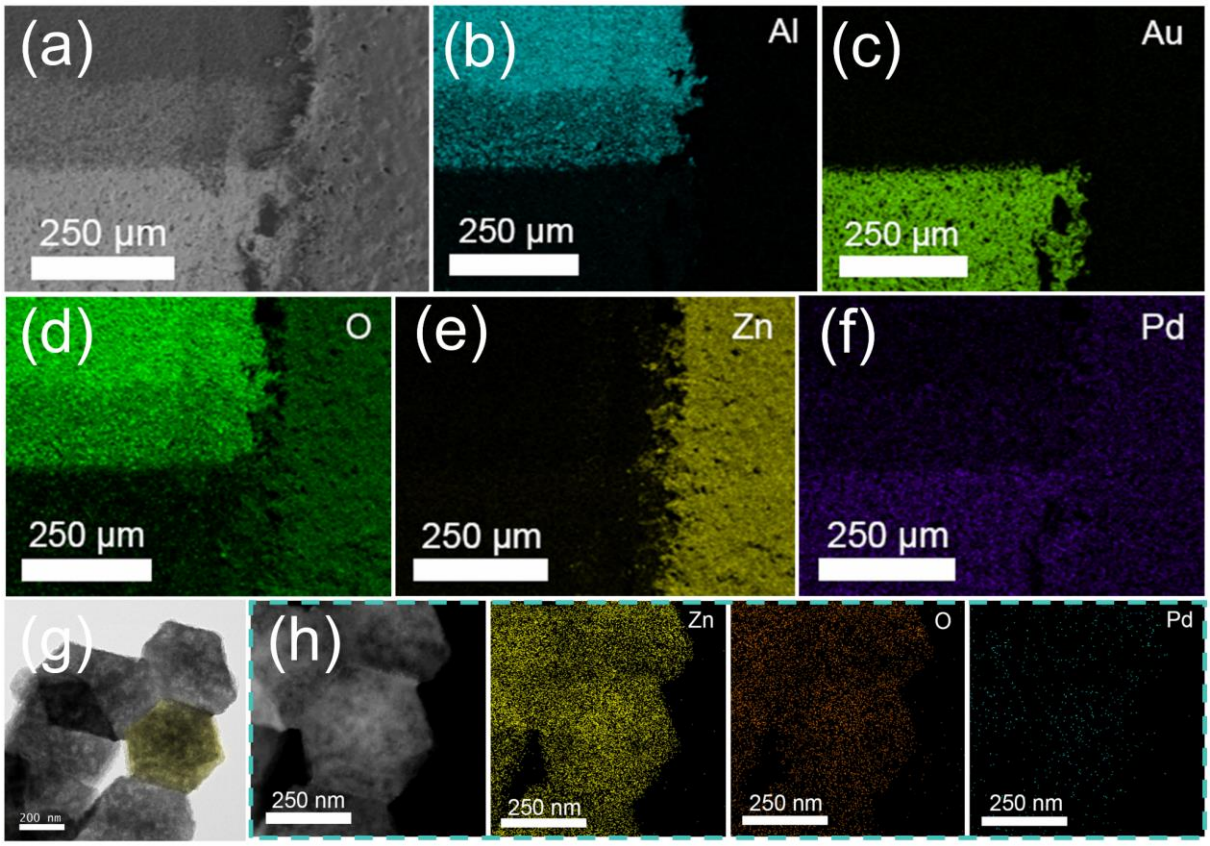

Figure S5. Characterizations of the porous thin film on the fabricated sensors. a) SEM images of 5.0Pd@ZnO porous thin film on Au-IDE (interdigitated electrodes) of the prepared sensor. b-f) Elemental mapping of porous thin film on Au-IDE. Characterization images of the MOF-derived porous nanocomposites: g) TEM image, and h) elemental mapping patterns.

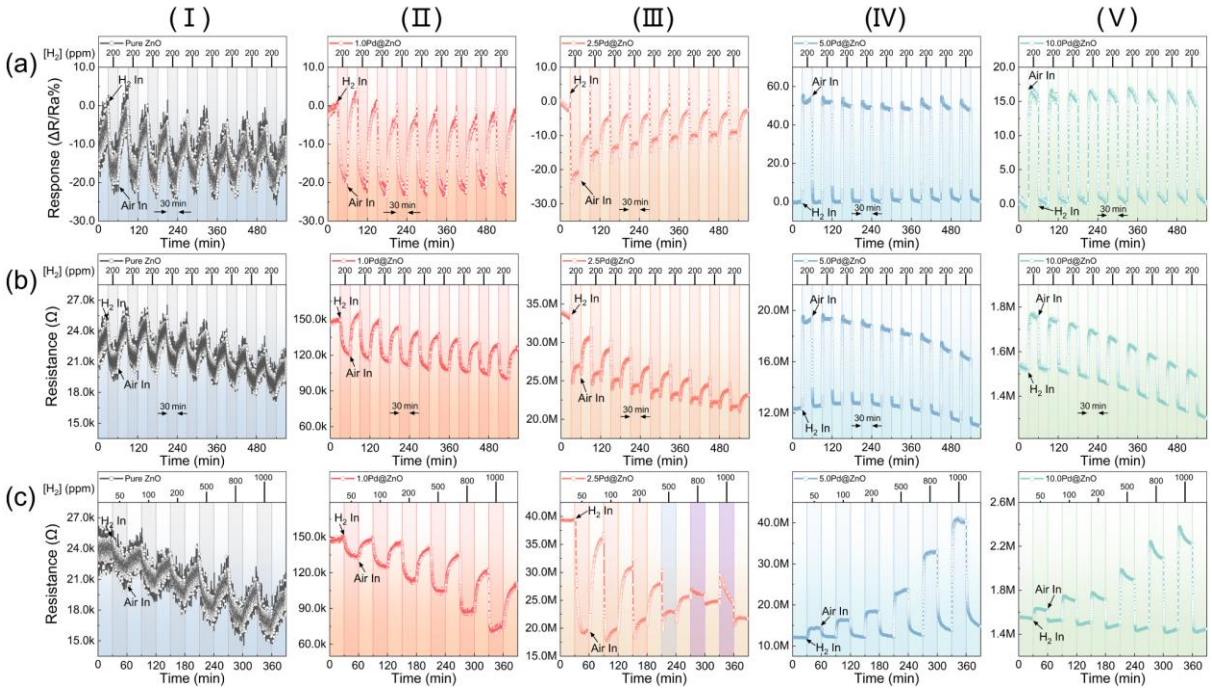

Figure S6. H_2 response properties of the sensors based on MOF-derived xPd@ZnO nanocomposites at room temperature. a_I-a_V) Reversibility of the as-prepared sensors toward 200 ppm H_2 under UV irradiation. b_I-b_V) Resistance reversibility of the as-prepared sensors toward 200 ppm H_2 under UV irradiation. c_I-c_V) Resistance transients of as-prepared sensors to different concentrations of 50-1000 ppm H_2 under UV irradiation.

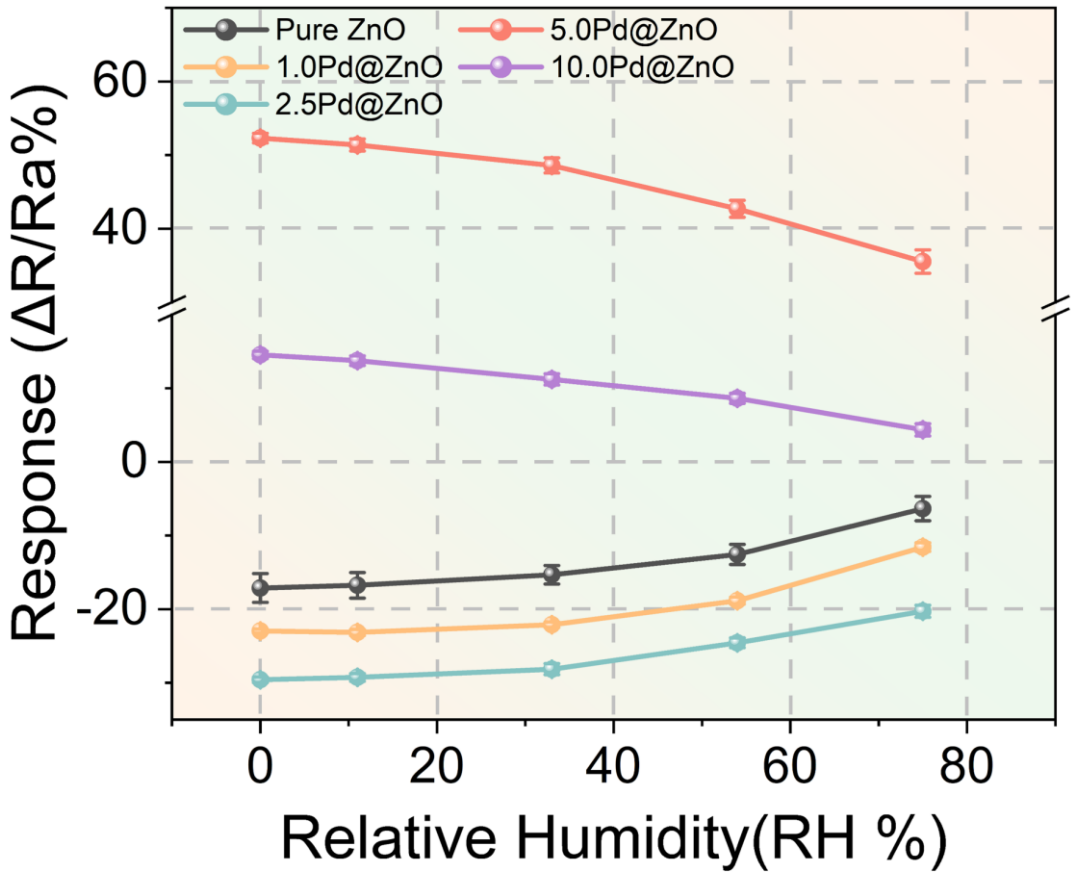

Figure S7. Influence of relatively humidity (RH) on the response of MOF-derived xPd@ZnO porous nanocomposites to 200 ppm H_2 at room temperature.

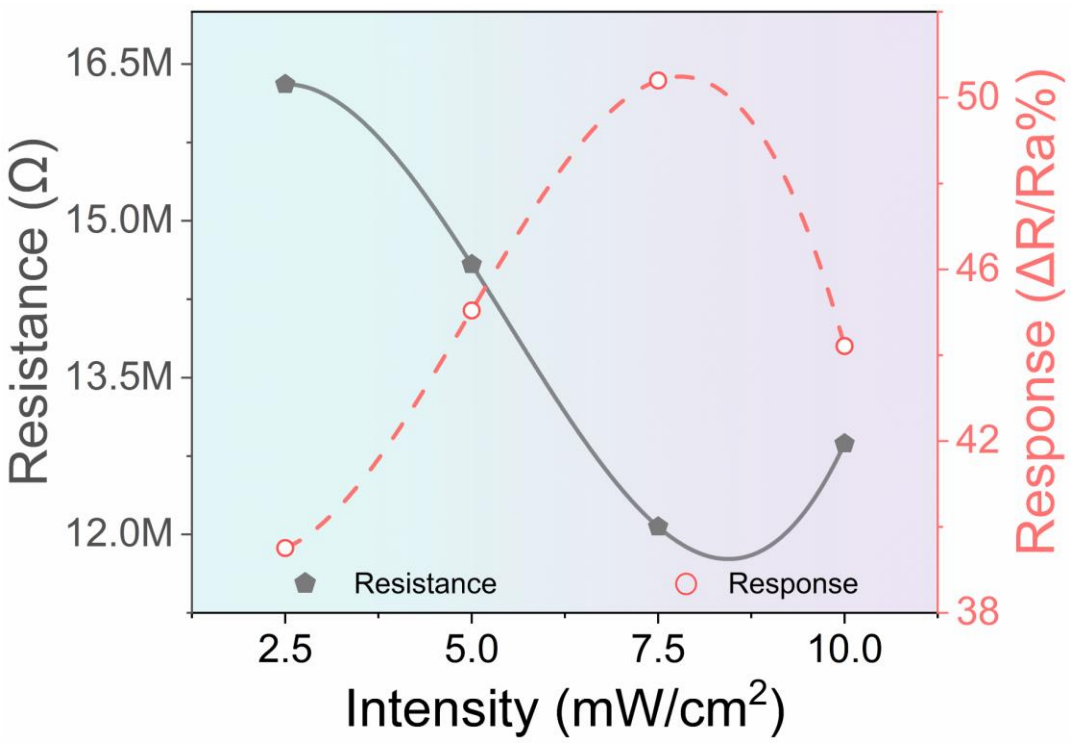

Figure S8. Effects of different UV intensities on resistance and response of MOF-derived 5.0Pd@ZnO.

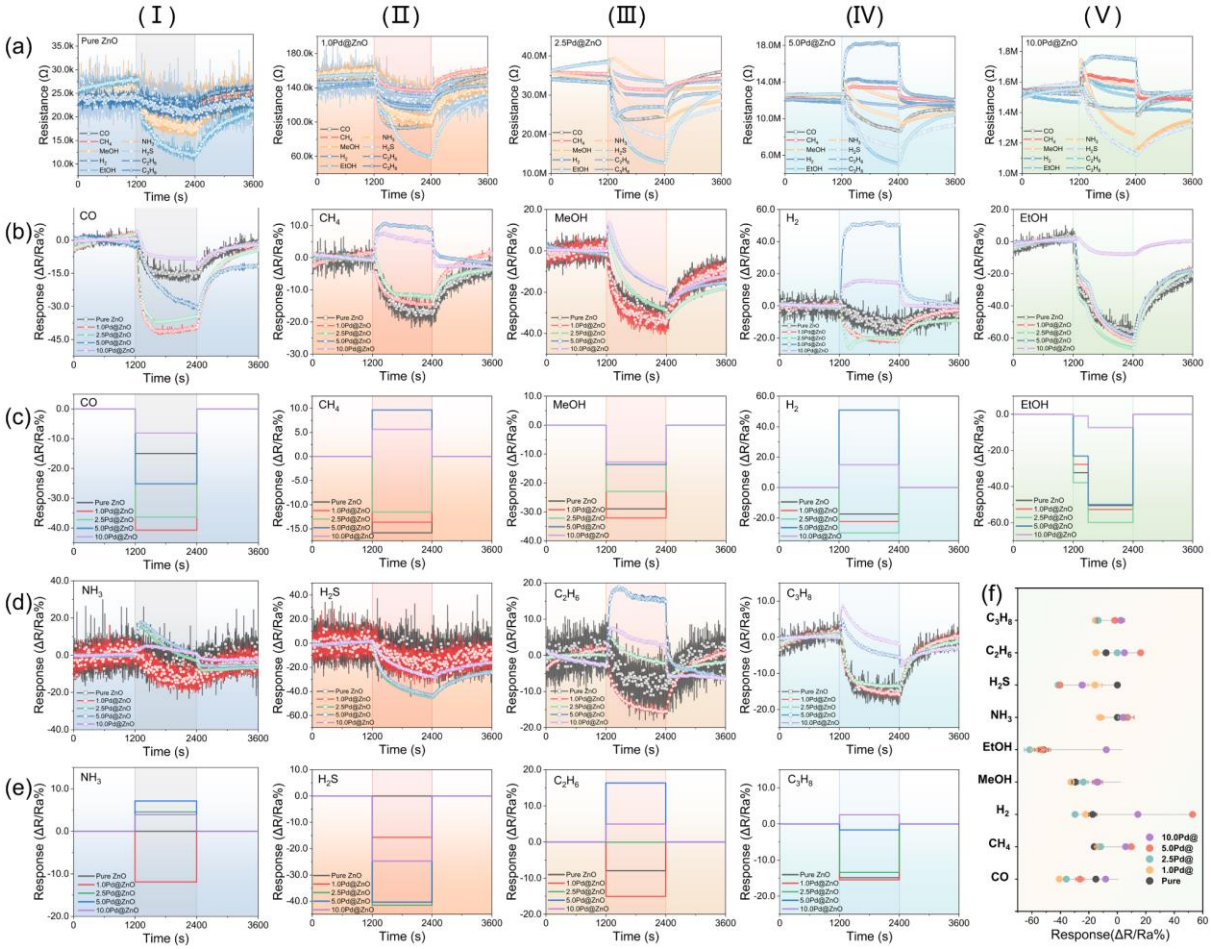

Figure S9. Selectivity tests of sensors based on MOF-derived xPd@ZnO nanocomposites to different typical flammable gases (CO, $C_xH_{2x+2,\ x\leq3}$, H_2, MeOH, EtOH, NH_3, H_2S) with a concentration of 200 ppm at room temperature. a_I-a_V) Resistance transients comparison of different as-prepared sensors to each flammable gas. b_I-b_V, d_I-d_{IV}) Response transient comparison of different as-prepared sensors for a single gas, and c_I-c_V, e_I-e_{IV}) the corresponding impulse response curves. f) Response preference of each sensor to a single flammable gas.

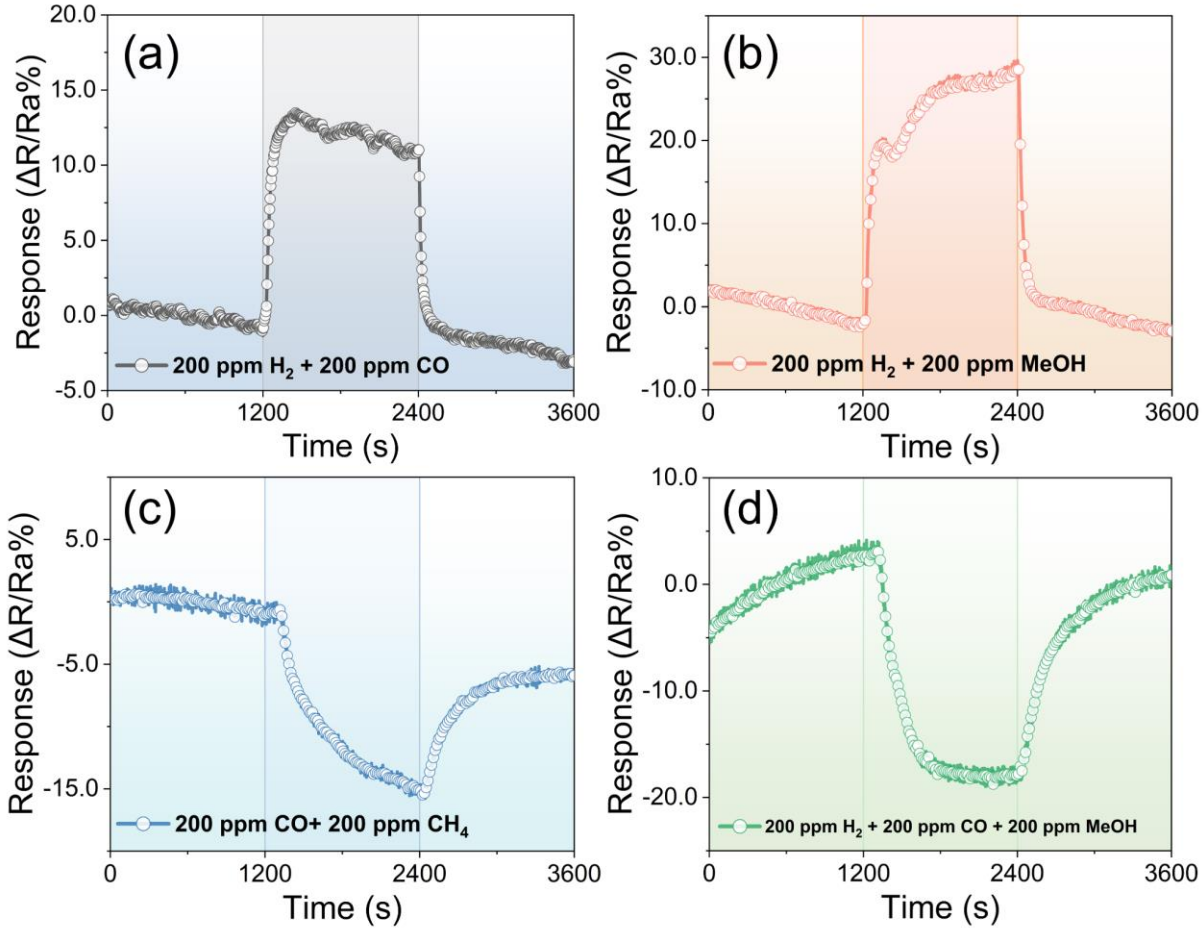

Figure S10. Sensing characterization tests of the as-prepared sensors in complex environment with multi-gases. Response transients of the 5.0Pd@ZnO nanocomposites in the mixed gases atmosphere of a) H_2 (200 ppm) and CO (200 ppm); b) H_2 (200 ppm) and MeOH (200 ppm); c) CO (200 ppm) and CH_4 (200 ppm); and d) H_2 (200 ppm), CO (200 ppm), and MeOH (200 ppm).

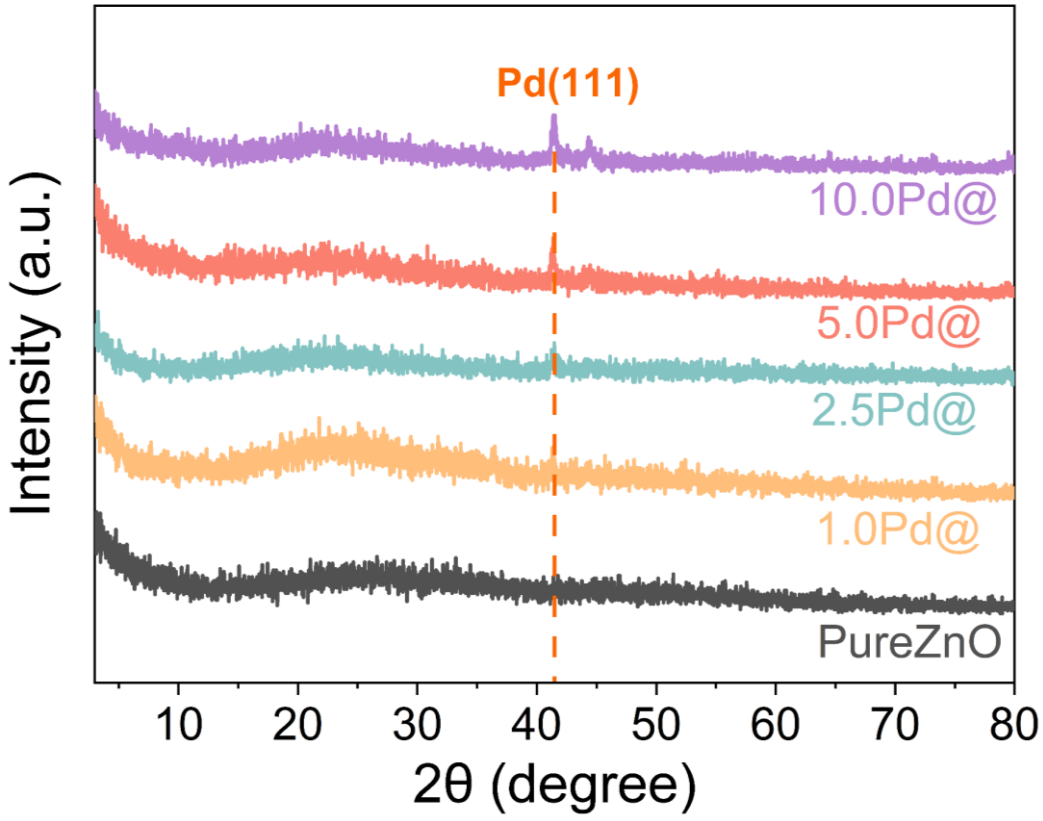

Figure S11. XRD patterns of ZIF-8 derived nanocomposites carbonized at 650 ℃ in Ar.

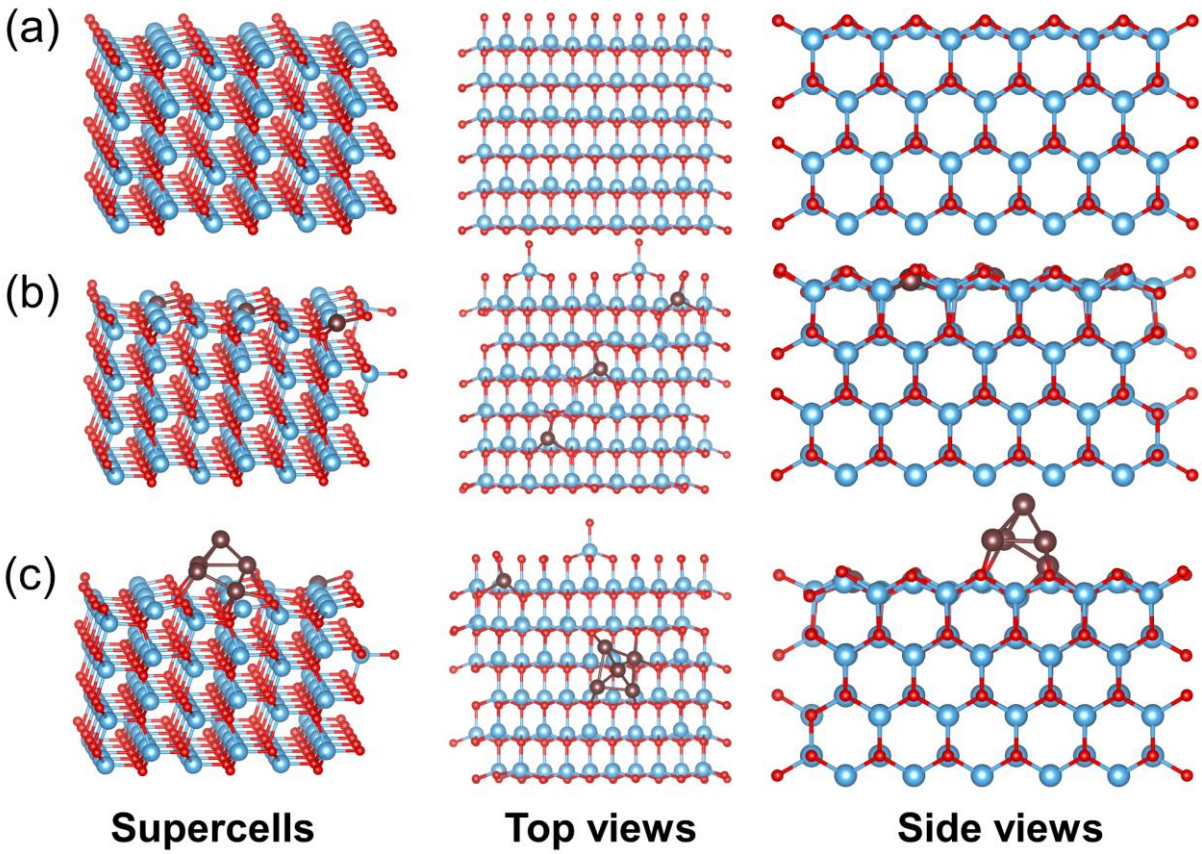

Figure S12. Top and side views of the optimized supercell configuration: a) pure ZnO, b) 2.5Pd@ZnO, and c) 5.0Pd@ZnO.

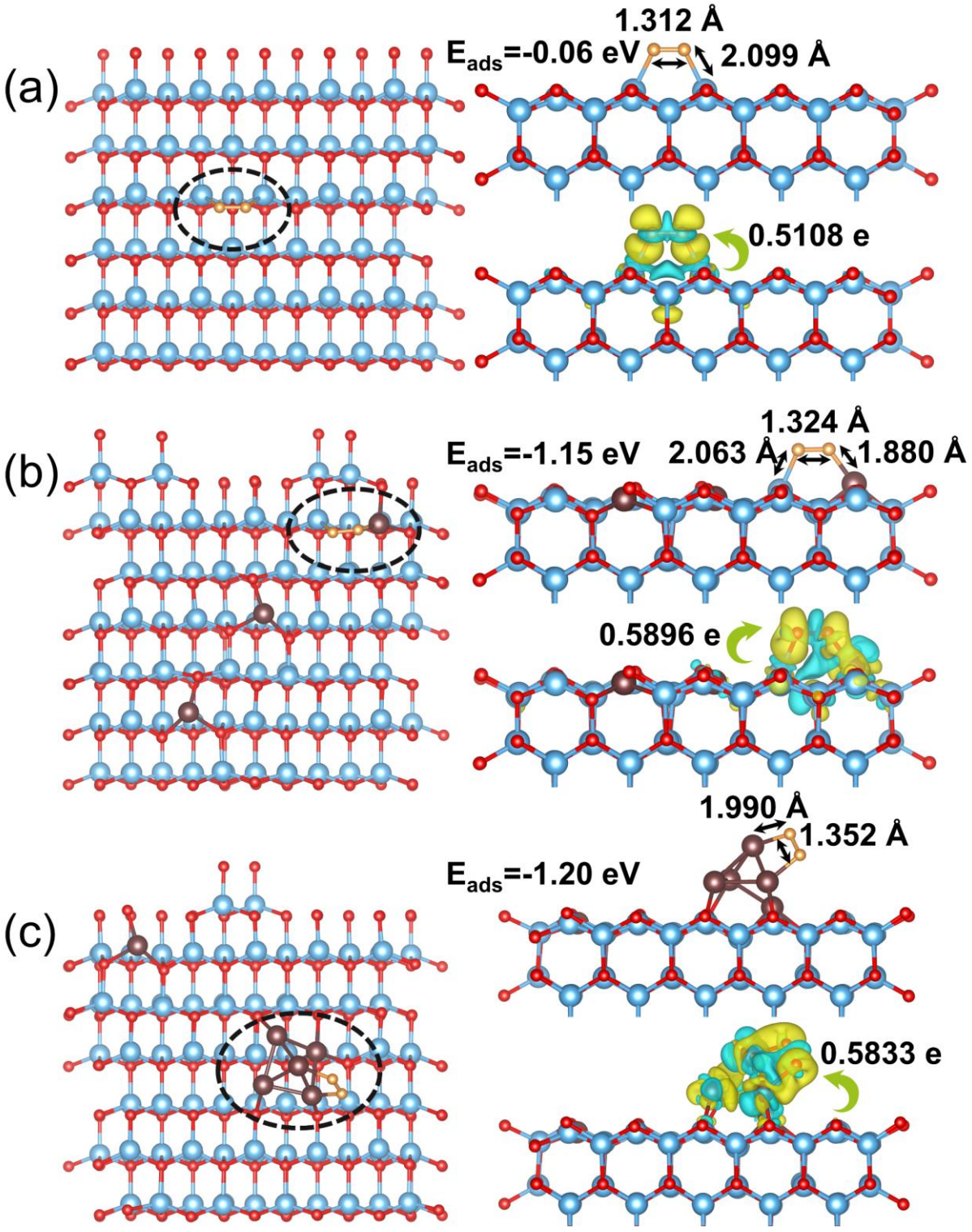

Figure S13. Adsorption characteristics and charge density difference of O_2 molecule in different configurations: a) pure ZnO, b) 2.5Pd@ZnO, and c) 5.0Pd@ZnO. The yellow and blue isosurfaces with an isosurface level of 0.0015e $Å^{-3}$ correspond to charge accumulation and depletion, respectively.

References

1. G. Kresse and D. Joubert, *Phys. Rev. B*, 1999, **59**, 1758.
2. J. P. Perdew, M. Ernzerhof and K. Burke, *J. Chem. Phys.*, 1996, **105**, 9982-9985.
3. P. E. Blochl, *Phys. Rev., B Condens. Matter*, 1994, **50**, 17953-17979.
4. W. Tang, E. Sanville and G. Henkelman, *J. Phys. Condens. Matter*, 2009, **21**, 084204.